Conduction gap in graphene strain junctions: direction dependence

2014 Semicond. Sci. Technol. 29 115024

(http://iopscience.iop.org/0268-1242/29/11/115024)

IOP Publishing Semiconductor Science and Technology
Semicond. Sci. Technol. **29** (2014) 115024 (10pp) doi:10.1088/0268-1242/29/11/115024

Conduction gap in graphene strain junctions: direction dependence

M Chung Nguyen[1,2], V Hung Nguyen[1,2,3], Huy-Viet Nguyen[2] and P Dollfus[1]

[1] Institut d'Electronique Fondamentale, UMR8622, CNRS, Université Paris Sud, 91405 Orsay, France
[2] Center for Computational Physics, Institute of Physics, Vietnam Academy of Science and Technology, PO Box 429 Bo Ho, 10000 Hanoi, Vietnam
[3] L_Sim, SP2M, UMR-E CEA/UJF-Grenoble 1, INAC, 38054 Grenoble, France

E-mail: hung@iop.vast.ac.vn

Received 17 July 2014, revised 27 August 2014
Accepted for publication 4 September 2014
Published 2 October 2014

Abstract

It has been shown in a recent study (Nguyen *et al* 2014 *Nanotechnology* **25** 165201) that unstrained/strained graphene junctions are promising candidates to improve the performance of graphene transistors which is usually hindered by the gapless nature of graphene. Although the energy bandgap of strained graphene still remains zero, the shift of Dirac points in the k-space due to strain-induced deformation of graphene lattice can lead to the appearance of a finite conduction gap of several hundred meV in strained junctions with a strain of only a few per cent. However, since it depends essentially on the magnitude of the Dirac point shift, this conduction gap strongly depends on the direction of applied strain and the transport direction. In this work, a systematic study of conduction-gap properties with respect to these quantities is presented and the results are carefully analyzed. Our study provides useful information for further investigations to exploit graphene-strained junctions in electronic applications and strain sensors.

Keywords: energy gap, graphene, strain, tight binding approach

1. Introduction

In spite of being an attractive material with excellent electronic properties [1], practical applications of graphene in conventional semiconductor devices are still questionable due to its gapless nature. In particular, the ON/OFF current ratio is low while the saturation of current is poor in pristine graphene transistors [2]. Many efforts of bandgap engineering in graphene [11–14, 16] have been made to solve these issues. The pioneer technique proposed [11] is to cut two-dimensional (2D) graphene sheets into one-dimensional (1D) narrow nanoribbons. In 2D graphene sheets, some options such as Bernal-stacking of graphene on hexagonal boron nitride substrate [12], nitrogen-doped graphene [13], graphene nanomesh lattice [14, 15] and Bernal-stacking bilayer graphene [16] have been explored. However, the possibility to open a sizable bandgap in graphene as large as those of standard semiconductors is still very unlikely. In particular, it requires very good control of lattice geometry and edge disorder in narrow graphene nanoribbons (GNRs) [17] and in graphene nanomesh lattices [18], while the bandgap opening in bilayer graphene by a perpendicular electric field may not be large enough for realistic applications [19]. Other methods should be further verified by experiments.

On the other hand, graphene was experimentally demonstrated to be able to sustain a much larger strain than conventional semiconductors, making it a promising candidate for flexible electronics (see in a recent review [20]). For instance, a graphene sheet on an unstretched polydimethylsiloxane substrate can endure and show good recovery of sheet resistance after 6% stretching [21]. On a pre-stretched polydimethylsiloxane substrate, graphene even showed stable sheet resistance up to 11%, and there was only one order change in this resistance up to 25% stretching. Especially, there are two recent works [22, 23] demonstrating techniques to generate extreme strains (>10%) in graphene in a controlled and nondestructive way. Garza *et al* [22] demonstrated the generation of uniaxial strains by pulling graphene using a tensile-MEMS while Shioya *et al* [23] achieved both biaxial strained and isotropic compressive strained states of graphene using thin-film-shrinkage methods. Interestingly, strain engineering has been suggested to

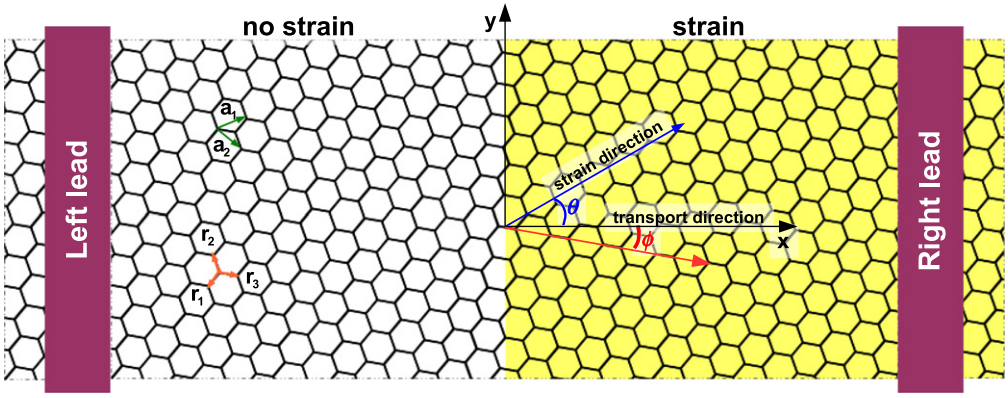

Figure 1. Schematic of unstrained/strained graphene junctions investigated in this work.

be an alternative approach to modulating efficiently the electronic properties of graphene nanomaterials [24]. In particular, the bandgap has periodic oscillations in the armchair GNRs [25], while the spin polarization at the ribbon edges (and also the bandgap) can be modulated by the strain in the zigzag cases. In 2D graphene sheets, a finite gap can open under large strains; otherwise, it can remain close to zero but the Dirac points are displaced [24, 26–29]. Many interesting electrical, optical, and magnetic properties induced by strain in graphene have been also explored; e.g. see [24, 30–38].

In addition, local strain is a good option to improve the electrical performance of graphene devices [24, 39–42]. For instance, it has been shown to enhance the ON current in a GNR-tunneling field effect transistor [39] and to fortify the transport gap in GNR-strained junctions [42]. In a recent work [43], we investigated the effects of uniaxial strain on the transport in 2D unstrained/strained graphene junctions and found that due to the strain-induced shift of Dirac points, a significant conduction gap of a few hundred meV can open with a small strain of a few percent. Note that the mentioned conduction gap is the energy window within which the Fermi energy can be varied and the junction remains insulating. This type of strained junction was then demonstrated to be an excellent candidate to improve the electronic operation of graphene transistors. Hence, it motivates us to further investigate the properties of this conduction gap so as to optimize the performance of graphene devices. On the one hand, the effects of strain should be, in principle, dependent on its applied direction. On the other hand, as a consequence of the shift of Dirac points along the perpendicular axis, the conduction gap is predicted to depend also on the transport direction. These properties of the conduction gap will be clarified fully in the current work.

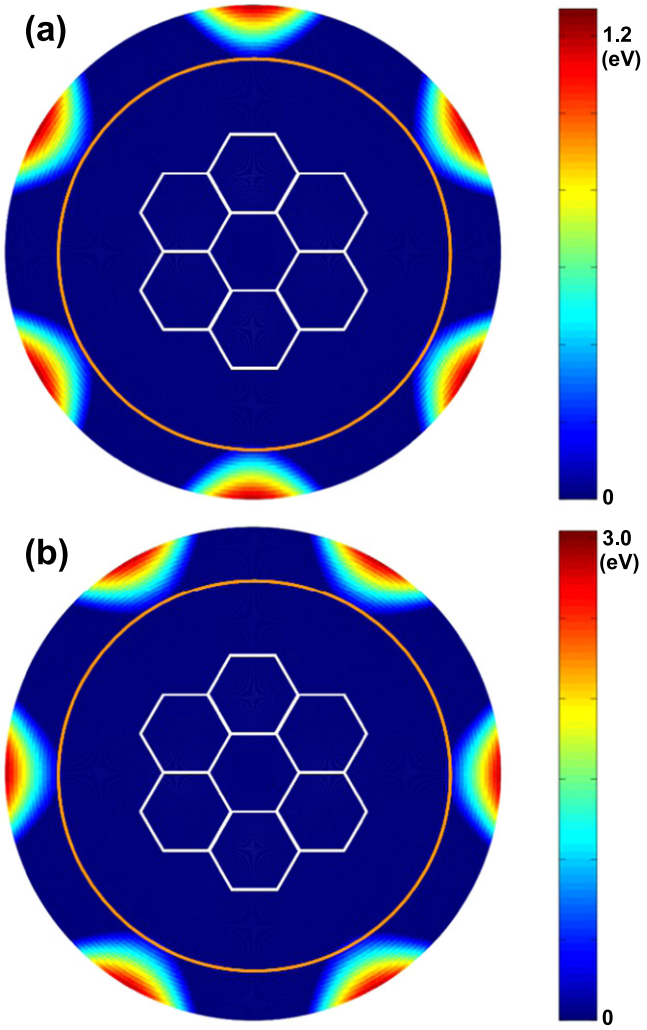

Figure 2. Dependence of graphene bandgap on the applied strain and its direction: tensile (a) and compressive (b). The radius from the central point indicates strain strength ranging from 0 (center) to 30% (edge of maps), while the graphene lattice is superimposed to show visibly the strain direction. The orange circle corresponds to the strains of $\sigma = 23\%$.

2. Model and calculations

In this work, the π-orbital tight-binding model constructed in [27] is used to investigate the electronic transport through the graphene-strained junctions schematized in figure 1, where the strain is applied to one half of a 2D graphene sheet as in [43]. The Hamiltonian is $H_{tb} = \sum_{nm} t_{nm} c_n^{\dagger} c_m$, where t_{nm} is the hopping energy between nearest neighbor nth and mth atoms. The application of a uniaxial strain of angle θ causes the

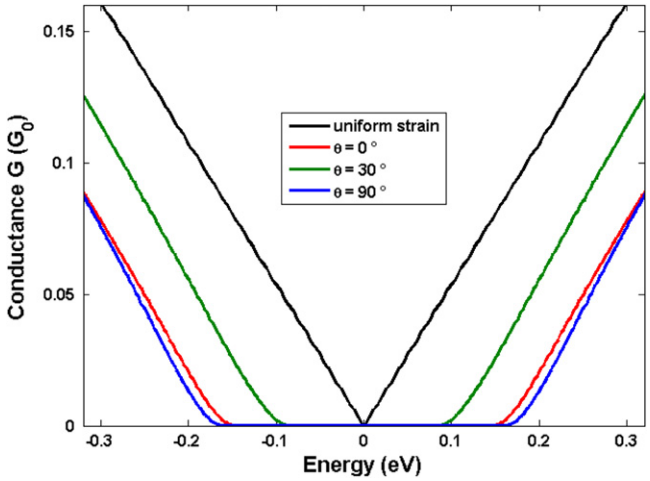

Figure 3. Conductance ($G_0 = e^2W/hL_y$) as a function of energy in graphene-strained junctions for $\sigma = 4\%$ with different strain directions. The transport along the armchair direction ($\phi = 0$) is considered. The data obtained in a uniformly strained graphene is displayed for the comparison.

following changes in the $C - C$ bond vectors:

$$\vec{r}_{nm}(\sigma) = \{1 + M_s(\sigma, \theta)\}\vec{r}_{nm}(0)$$
$$M_s(\sigma, \theta) = \sigma \begin{bmatrix} \cos^2\theta - \gamma \sin^2\theta & (1+\gamma)\sin\theta\cos\theta \\ (1+\gamma)\sin\theta\cos\theta & \sin^2\theta - \gamma\cos^2\theta \end{bmatrix} \quad (1)$$

where σ represents the strain and $\gamma \simeq 0.165$ is the Poisson ratio [44]. The hopping parameters are defined as $t_{nm}(\sigma) = t_0 \exp[-3.37(r_{nm}(\sigma)/r_0 - 1)]$, where the hopping energy $t_0 = -2.7$ eV and the bond length $r_{nm}(0) \equiv r_0 = 0.142$ nm in the unstrained case. Therefore, there are three different hopping parameters $t_{1,2,3}$ corresponding to three bond vectors $\vec{r}_{1,2,3}$, respectively, in the strained graphene part of the structure (see figure 1). Here, we investigate a 2D graphene channel, i.e., the lateral size W (along the Oy direction) of the graphene sheet is much larger than the length (along the Ox direction and, e.g., $\sim$ a few tens of nm, as studied in [43]) of the active region. We assume a 1D profile of applied strain, i.e., the strain tensor, is a function of position along the transport direction while it is constant along the perpendicular one. Note that here, Ox (resp. Oy)—axis is parallel (resp. perpendicular) to the transport direction. The transport direction, ϕ, and strain direction, θ, are determined as schematized in figure 1. Based on this tight-binding model, the two methods described below can be used to investigate the conduction gap of strained junctions.

Green's function calculations. First, we split the graphene sheet into the smallest possible unit cells periodically repeated along the Ox/Oy directions with the indices p/q, respectively (similarly, see the details in [45]). The tight-binding Hamiltonian can therefore be expressed in the following form:

$$H_{tb} = \sum_{p,q}\left(H_{p,q} + \sum_{p_1,q_1} H_{p,q\to p_1,q_1}\right), \quad (2)$$

where $H_{p,q}$ is the Hamiltonian of cell $\{p, q\}$, and $H_{p,q\to p_1,q_1}$ denotes the coupling of cell $\{p, q\}$ to its nearest neighbor cell $\{p_1, q_1\}$. We then Fourier transform the operators in equation (2) as follows:

$$c_{p,q} = \frac{1}{\sqrt{M_{cell}}}\sum_{\kappa_y} e^{iq\kappa_y}\hat{c}_{p,\kappa_y}, \quad (3)$$

where M_{cell} is the number of unit cells and $\kappa_y \equiv k_y L_y$ with the size L_y of unit cells along the Oy direction. The Hamiltonian (2) is finally rewritten as a sum of κ_y-dependent 1D components:

$$H_{tb} = \sum_{\kappa_y}\hat{H}(\kappa_y)$$
$$\hat{H}(\kappa_y) = \sum_{p}\hat{H}_{p\to p-1}(\kappa_y) + \hat{H}_p(\kappa_y) + \hat{H}_{p\to p+1}(\kappa_y) \quad (4)$$

With the Hamiltonian in this form, the non-equilibrium Green's function formalism can easily be applied to compute transport quantities in the graphene-strained junction with different transport directions. In particular, the conductance at zero temperature is determined as:

$$\mathcal{G}(\epsilon_F) = \frac{e^2W}{\pi h L_y}\int_{BZ} d\kappa_y \mathcal{T}(\epsilon_F, \kappa_y), \quad (5)$$

where $W \equiv M_{cell}L_y$ and $\mathcal{T}(\epsilon_F, \kappa_y)$ is the transmission probability computed from the Green's functions. The integration over κ_y is performed in the first Brillouin zone. As in [18], the gap of conductance (conduction gap) is then measured from the obtained data of conductance.

Bandstructure analysis. To determine the conduction gap of strained junctions, we find that another simple way based on the analysis of graphene bandstructures could be efficiently used. It is described as follows. Since the conductance is computed from equation (5), the appearance of a conduction gap is essentially governed by the gaps of transmission probability, which is determined from the energy gaps in the unstrained and strained graphene sections. These energy gaps can be defined directly from the graphene bandstructures. Therefore, our calculation has two steps, similar to that in [43]. From the graphene bandstructures obtained using the tight-binding Hamiltonian above, we first look for the energy gaps $E^{gap}_{unstrain}(\kappa_y)$ and $E^{gap}_{strain}(\kappa_y)$ for a given κ_y of two graphene sections. The maximum of these energy gaps determines the gap $E^{gap}_{junc}(\kappa_y)$ of transmission probability through the junction. Finally, the conduction gap $E_{cond.gap}$ is obtained by looking for the minimum value of $E^{gap}_{junc}(\kappa_y)$ when varying κ_y in the whole Brillouin zone.

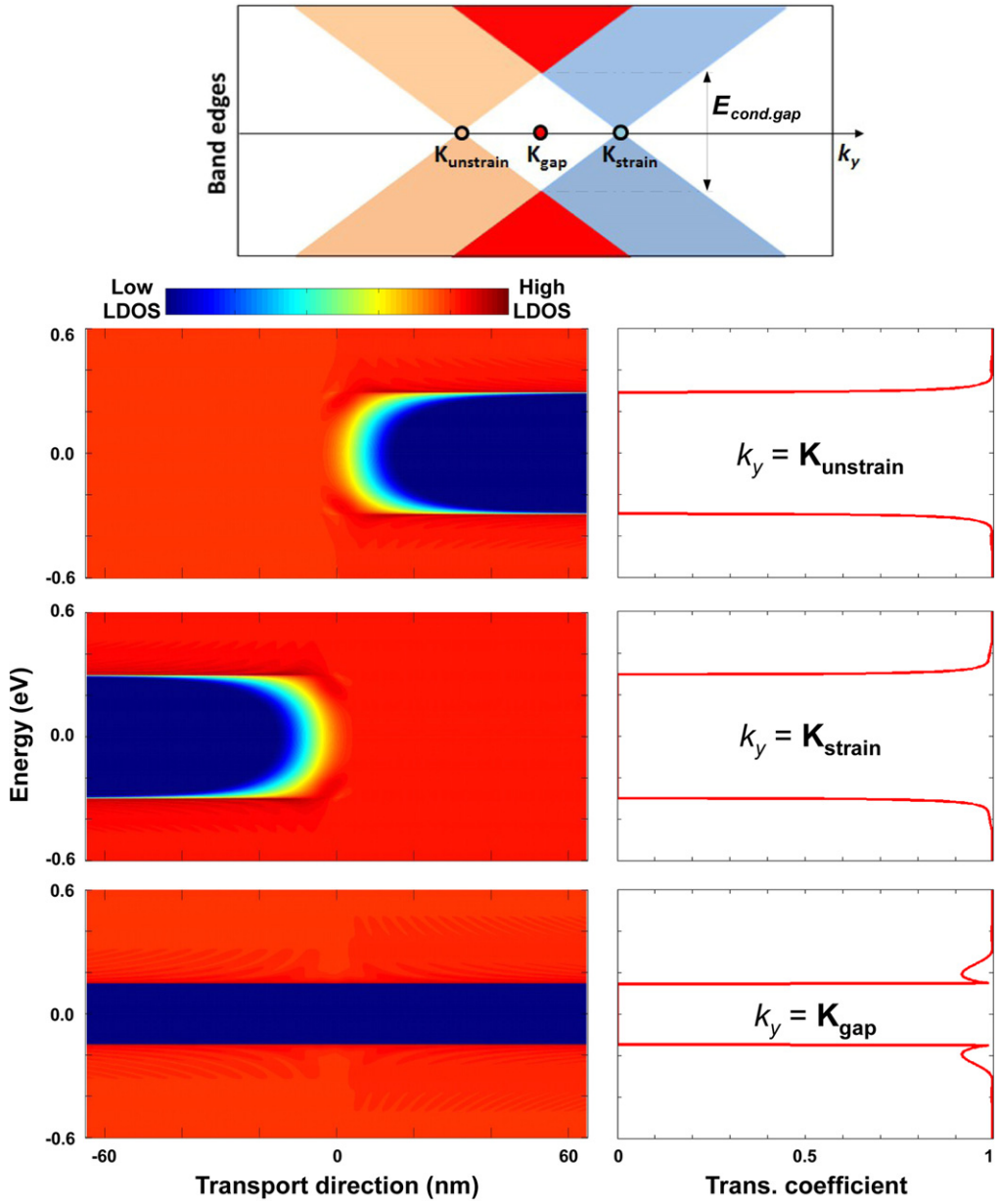

Figure 4. Local density of states (left panels) and corresponding transmission coefficient (right panels) for three different wave-vectors k_y obtained in an unstrained/strained graphene junction of $\sigma = 4\%$, and $\theta \equiv \phi = 0$. On the top is a schematic of graphene bandedges illustrating the strain-induced shift of Dirac points along the k_y-direction.

In particular, the energy bands of strained graphene are given by

$$E(\vec{k}) = \pm |t_1 e^{i\vec{\mathbf{k}}\cdot\vec{\mathbf{a}}_1} + t_2 e^{i\vec{\mathbf{k}}\cdot\vec{\mathbf{a}}_2} + t_3|, \tag{6}$$

where the plus/minus sign corresponds to the conduction/valence bands, respectively. For a given direction ϕ of transport, in principle, the vectors $\vec{\mathbf{L}}_{\mathbf{x,y}}$ defining the sizes of unit cells along the Ox and Oy directions, respectively, can be always expressed as $\vec{\mathbf{L}}_{\mathbf{x}} = n_1\vec{\mathbf{a}}_{\mathbf{1}} + n_2\vec{\mathbf{a}}_{\mathbf{2}}$ and $\vec{\mathbf{L}}_{\mathbf{y}} = m_1\vec{\mathbf{a}}_{\mathbf{1}} + m_2\vec{\mathbf{a}}_{\mathbf{2}}$ with $\cos\phi = \frac{\vec{\mathbf{L}}_x\cdot\vec{\mathbf{L}}_x^{\mathbf{0}}}{\|\vec{\mathbf{L}}_x\|\|\vec{\mathbf{L}}_x^{\mathbf{0}}\|}$ and $\sin\phi = \frac{\vec{\mathbf{L}}_x\cdot\vec{\mathbf{L}}_y^{\mathbf{0}}}{\|\vec{\mathbf{L}}_x\|\|\vec{\mathbf{L}}_y^{\mathbf{0}}\|}$ while $\vec{\mathbf{L}}_{x,\,y}^{\mathbf{0}} = \vec{\mathbf{a}}_{\mathbf{1}} \pm \vec{\mathbf{a}}_{\mathbf{2}}$. Note that $n_{1,2}$ and $m_{1,2}$ are integers, while $\frac{m_1}{m_2} = -\frac{n_1+2n_2}{n_2+2n_1}$, i.e., $\vec{\mathbf{L}}_{\mathbf{x}}\cdot\vec{\mathbf{L}}_{\mathbf{y}} = 0$. In other words, we have the following expressions

$$\vec{\mathbf{a}}_{\mathbf{1}} = \frac{-m_2\vec{\mathbf{L}}_{\mathbf{x}} + n_2\vec{\mathbf{L}}_{\mathbf{y}}}{n_2m_1 - n_1m_2};\ \vec{\mathbf{a}}_{\mathbf{2}} = \frac{m_1\vec{\mathbf{L}}_{\mathbf{x}} - n_1\vec{\mathbf{L}}_{\mathbf{y}}}{n_2m_1 - n_1m_2}. \tag{7}$$

On this basis, the energy bands can be rewritten in terms of $\kappa_{x,y} = \vec{\mathbf{k}}\cdot\vec{\mathbf{L}}_{\mathbf{x,y}}(\equiv k_{x,y}L_{x,y})$ by substituting equations (7) into (6). This new form of energy bands is finally used to compute the conduction gap of strained junctions.

As a simple example, in the case of $\phi = 0$ (armchair direction), we calculate the conduction gap as follows. First, equation (6) is rewritten in the form

$$E_{\phi=0}(\vec{\kappa}) = \pm |t_1 e^{i\kappa_y/2} + t_2 e^{-i\kappa_y/2} + t_3 e^{-i\kappa_x/2}| \tag{8}$$

with the vectors $\vec{\mathbf{L}}_{\mathbf{x,y}} \equiv \vec{\mathbf{L}}_{\mathbf{x},\,\mathbf{y}}^{\mathbf{0}}$. Using this new form, the energy

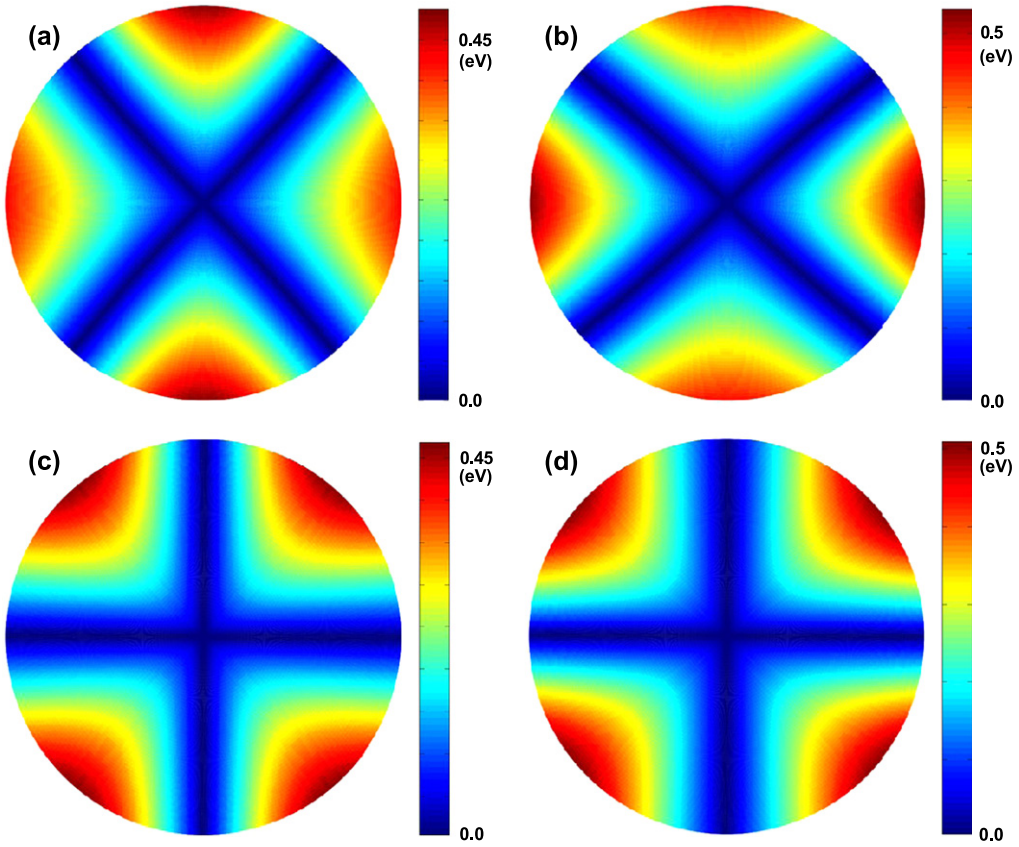

Figure 5. Maps of conduction gap in unstrained/strained graphene junctions: tensile (a, c) and compressive cases (b, d). The transport is along the armchair $\phi = 0$ (a, b) and zigzag $\phi = 30°$ directions (c, d). The strain strength ranges from 0 (center) to 6% (edge of maps) in all cases.

gap of strained graphene for a given κ_y is determined as

$$E^{gap}_{strain}(\kappa_y) = 2\left|\sqrt{(t_1 - t_2)^2 + 4t_1t_2\cos^2\frac{\kappa_y}{2}} + t_3\right| \quad (9)$$

while $E^{gap}_{unstrain}(\kappa_y)$ is given by the same formula with $t_1 = t_2 = t_3 \equiv t_0$. The gap of transmission probability through the junction is then determined as $E^{gap}_{junc}(\kappa_y)$= max $[E^{gap}_{unstrain}(\kappa_y), E^{gap}_{strain}(\kappa_y)]$ and, finally, the conduction gap is given by $E_{cond.gap} = \min [E^{gap}_{junc}(\kappa_y)]$ for κ_y in the whole Brillouin zone.

Note that beyond the energy gaps mentioned, transmission through the junctions also depends on the size of the transition zone between unstrained and strained graphene sections. As shown in [42, 43], a short (i.e., smaller than about 5–6 nm) transition zone can have significant effects on the transmission probability; i.e., it can be slightly degraded compared to the case of junctions with a long transition zone. In this work, we mainly focus on the properties of the conduction gap with the assumption that the transition zone is long and hence the mentioned effect is negligible.

3. Results and discussion

First, we re-examined the formation of the bandgap of graphene under a uniaxial strain. From equation (9), it is shown that a strain-induced finite-bandgap appears only if $E^{gap}_{strain}(\kappa_y) > 0$ for all k_y in the first Brillouin zone, i.e., $k_y \in [-\frac{\pi}{L_y}, \frac{\pi}{L_y}]$; otherwise, the bandgap remains zero. Hence, the condition for the bandgap to be finite is either

$$|t_1 - t_2| > |t_3| \quad \text{OR} \quad |t_3| > |t_1 + t_2|,$$

and the corresponding values of the bandgap are

$$E_{gap} = 2\big(|t_1 - t_2| - |t_3|\big) \quad \text{OR} \quad 2\big(|t_3| - |t_1 + t_2|\big)$$

This result was actually reported in [27, 46]. We remind that, as displayed in figure 2(a), a finite bandgap opens only for strains larger than ~23% and the zigzag (not armchair) is the preferred direction for bandgap opening under a tensile strain [27]. We extend our investigation to the case of compressive strain and find [see in figure 2(b)] that (i) the same gap threshold of $\sigma \simeq 23\%$ is observed but (ii) the preferred direction to open the gap under a compressive strain is the armchair, not the zigzag, as is the case of tensile strain. This implies that the properties of graphene bandstructure at low energy should be qualitatively the same when applying strains of $\{\sigma, \theta\}$ and of $\{-\sigma, \theta + 90°\}$. This feature can be understood by considering, for example, strains of $\{\sigma, \theta = 0\}$ and of $\{-\sigma, \theta = 90°\}$. Indeed, these strains result in the same qualitative changes on the bond-lengths, i.e., an increased bond-length r_3 and reduced bond-lengths $r_{1,2}$. However, for the same strain strength, because of the exponential

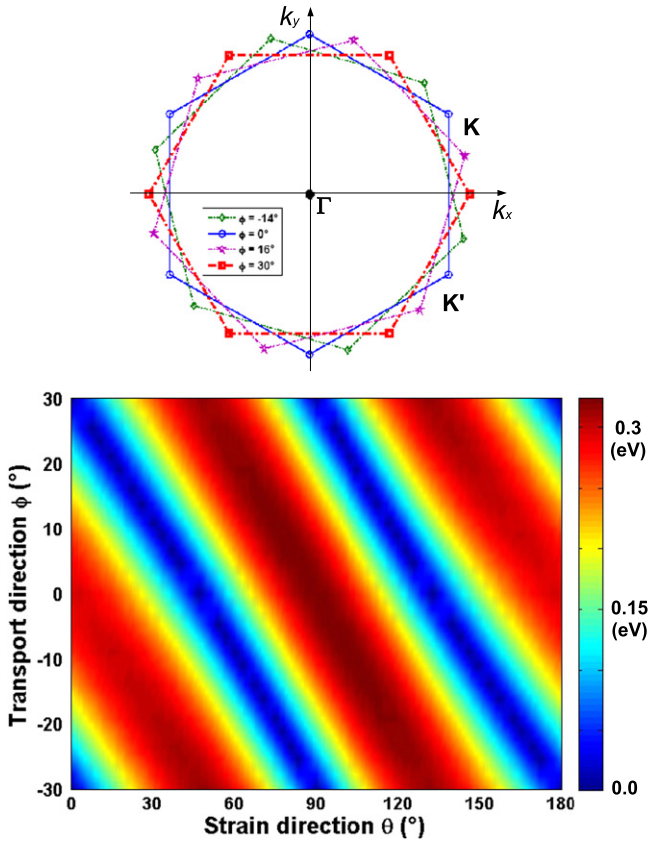

Figure 6. Map showing the dependence of conduction gap on the directions (θ, ϕ) for $\sigma = 4\%$. The top is a diagram illustrating the rotation of Dirac points in the k-space with the change in the transport direction ϕ.

dependence of hopping energies on the bond-lengths, the compressive strain generally induces a larger bandgap than the tensile one, as can be seen when comparing the data displayed in figures 2(a) and (b). We would like to emphasize again that a large strain is necessary to open a bandgap in graphene. This could be an issue for practical applications, compared to the use of graphene-strained junctions proposed in [43].

We now go to explore the properties of the conduction gap in graphene-strained junctions. In figure 3, we display the conductance as a function of energy computed from equation (5) using the Green's function technique. As discussed above, a small strain of a few percent (e.g., 4% here) cannot change the gapless character of graphene, i.e., there is no gap of conductance in the case of uniformly strained graphene though Dirac points are displaced as experimentally demonstrated in [28, 29]. However, similar to the result reported in [43], a significant conduction-gap of a few hundreds meV can open in the unstrained/strained graphene junctions. The appearance of this conduction gap, as mentioned previously, is due to the strain-induced shift of Dirac points in a mechanism described as follows. Actually, the bandedges as a function of wave-vector k_y in unstrained and strained graphene can be illustrated schematically in the top panel of figure 4. As one can see, the shift of Dirac points in strained graphene leads to a situation where there is no value of κ_y, for which the energy gaps $E^{gap}_{unstrain}(\kappa_y)$ and $E^{gap}_{strain}(\kappa_y)$ are simultaneously equal to zero. This means that the transmission probability always shows a finite gap, $E^{gap}_{junc}(\kappa_y) = \max\,[E^{gap}_{unstrain}(\kappa_y), E^{gap}_{strain}(\kappa_y)]$, for any κ_y. In particular, these energy gaps are zero (or small) in the unstrained (resp. strained) graphene section, but are finite in the strained (resp. unstrained) one in the vicinity of Dirac point $k_y = K_{unstrain}$ (resp. K_{strain}). Accordingly, as illustrated in the pictures of local density of states in the left panels of figure 4 and reinforced in the corresponding transmission functions in the right panels, well-defined gaps $E^{gap}_{junc}(\kappa_y)$ of transmission are still obtained. Far from the values of k_y above, $E^{gap}_{unstrain}(\kappa_y)$ and $E^{gap}_{strain}(\kappa_y)$ are both finite (e.g., see the LDOS plotted for $k_y = K_{gap}$) and hence a finite gap of transmission also occurs. On this basis, a finite gap of conductance, which is determined using equation (5), is achieved as shown in figure 3. This gap is simply given by $E_{cond.gap} = \min\,[E^{gap}_{junc}(\kappa_y)]$ for all κ_y as discussed in the subsection 'bandstructure analysis' and visibly illustrated in the top panel of figure 4. More important, figure 3 shows that besides the strength of strain, the strain effect is also strongly dependent on the applied direction. For instance, the conduction gap takes the values of ~295, 172 and 323 meV for $\theta = 0, 30°$ and 90°, respectively.

Below, we will discuss the properties of the conduction gap with respect to the strain, its applied direction, and the direction of transport. Note that due to the lattice symmetry, the transport directions ϕ and $\phi + 60°$ are equivalent while the applied strain of angle θ is identical to that of $\theta + 180°$. Hence, the data obtained for ϕ ranging from $-30°$ to 30° and $\theta \in [0°, 180°]$ covers the properties of the conduction gap in all possibilities.

In figure 5, we present the maps of conduction gap with respect to the strain and its applied direction in two particular cases where the transport is either along the armchair ($\phi = 0$) or the zigzag ($\phi = 30°$) directions. Both tensile and compressive strains are considered. Let us first discuss the results obtained in the armchair case. Figures 5(a) and (b) show that (i) a large conduction gap of up to ~500 meV can open with a strain of 6% and (ii) again the conduction gap is strongly θ-dependent; in particular, its peaks occur at $\theta = 0$ or 90° while the gap is zero at $\theta \approx 47°$ and 133° for tensile strain and at $\theta \approx 43°$ and 137° for compressive strain. In principle, the conduction gap is larger if the shift of Dirac points in the k_y-axis is larger, as in previous discussion about figures 3 and 4. We notice that the strain-induced shifts can be different for the six Dirac points of graphene [47] and the gap is zero whenever one Dirac point is observed at the same κ_y in the two graphene sections. From equation (9), we find that the Dirac points are determined by the following set of equations:

$$\cos\frac{\kappa_y}{2} = \pm\frac{1}{2}\sqrt{\frac{t_3^2 - (t_1 - t_2)^2}{t_1 t_2}},$$

$$\cos\frac{\kappa_x}{2} = \frac{t_1 + t_2}{|t_3|}\cos\frac{\kappa_y}{2}, \quad \sin\frac{\kappa_x}{2} = \frac{t_2 - t_1}{|t_3|}\sin\frac{\kappa_y}{2},$$

which simplify into $\cos\frac{\kappa_y}{2} = \pm\frac{1}{2}$ and, respectively,

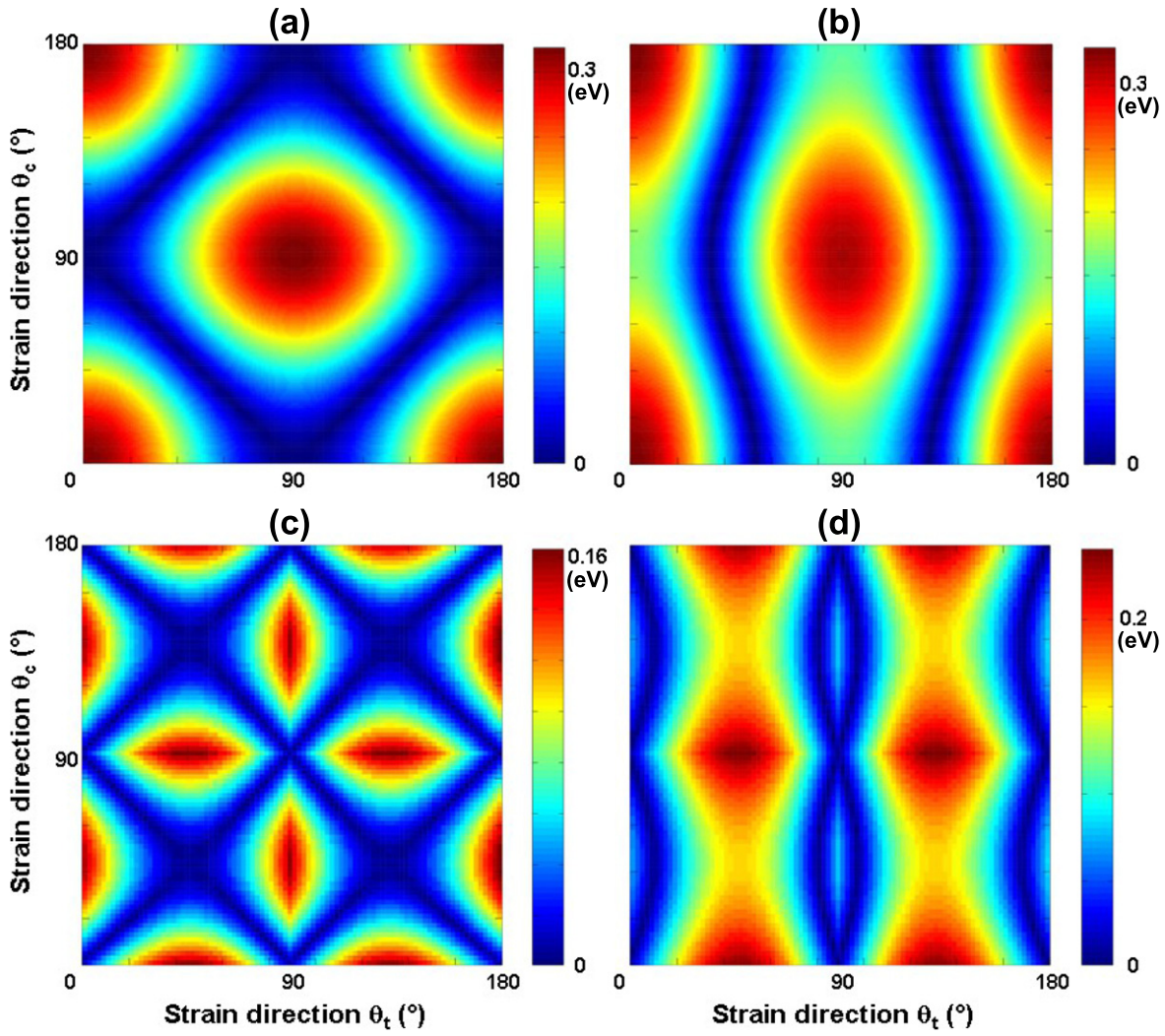

Figure 7. Maps of conduction gap obtained in tensile/compressive strained junctions. The transport along the armchair/zigzag directions is considered in (a, b)/(c, d), respectively. The strains $\sigma_c = -2\%$ and $\sigma_t = 2\%$ are applied in (a, c) while $\sigma_c = -1\%$ and $\sigma_t = 3\%$ in (b, d).

$\cos(\frac{\kappa_x}{2}) = \mp 1$ in the unstrained case. Hence, the zero conduction gap obtained above satisfies the condition

$$\frac{t_3^2 - (t_1 - t_2)^2}{4t_1t_2} = \frac{1}{4},$$

i.e., there is no shift of Dirac points along the κ_y-axis. Additionally, it is shown that the effects of a strain $\{\sigma, \theta\}$ are qualitatively similar to those of a strain $\{-\sigma, \theta + 90°\}$, i.e., the peaks and zero values of conduction gap are obtained at the same θ in these two situations. To understand this, we analyze the strain matrix $M_s(\sigma, \theta)$ and find that in the case of small strains studied here, the relationship between the bond lengths under these two strains is approximately given by

$$r(\sigma, \theta) - r(-\sigma, \theta + 90°) \simeq \sigma(1 - \gamma)r_0,$$

which is θ-independent for all C-C bond vectors. It implies that there is a fixed ratio between the hopping energies $t_i(\sigma, \theta)$ and $t_i(-\sigma, \theta + 90°)$ and hence a similar shift of Dirac points happens in these two cases.

Next, we analyze the properties of conduction gap displayed in figures 5(c) and (d) where the transport is along the zigzag direction $\phi = 30°$. In fact, the conduction gap in this case can also reach a value as high as that of the case of $\phi = 0$ but has different θ-dependence. In particular, the conduction gap has peaks at $\theta \approx 47°$ and 133° for tensile strain and at $\theta \approx 43°$ and 137° for compressive strain, where it is zero in the case of $\phi = 0$. It is also equal to zero at $\theta = 0$ and $\theta = 90°$ where the peaks of the conduction gap occur in the latter case of $\phi = 0$. The relationship between these two transport directions can be explained as follows. On the one hand, based on the analysis above for $\phi = 0$, we find that for a given strength of strain, a maximum shift of Dirac points along the k_y-axis corresponds to a minimum shift along the k_x-one and vice versa when varying the strain direction θ. On the other hand, as schematized in the top of figure 6, the change in transport direction results in the rotation of the first Brillouin zone, i.e., the k_x (resp. k_y) axis in the case of $\phi = 30°$ is identical to the k_y (resp. k_x) axis in the case of $\phi = 0$. These two features explain essentially the opposite θ-dependence of

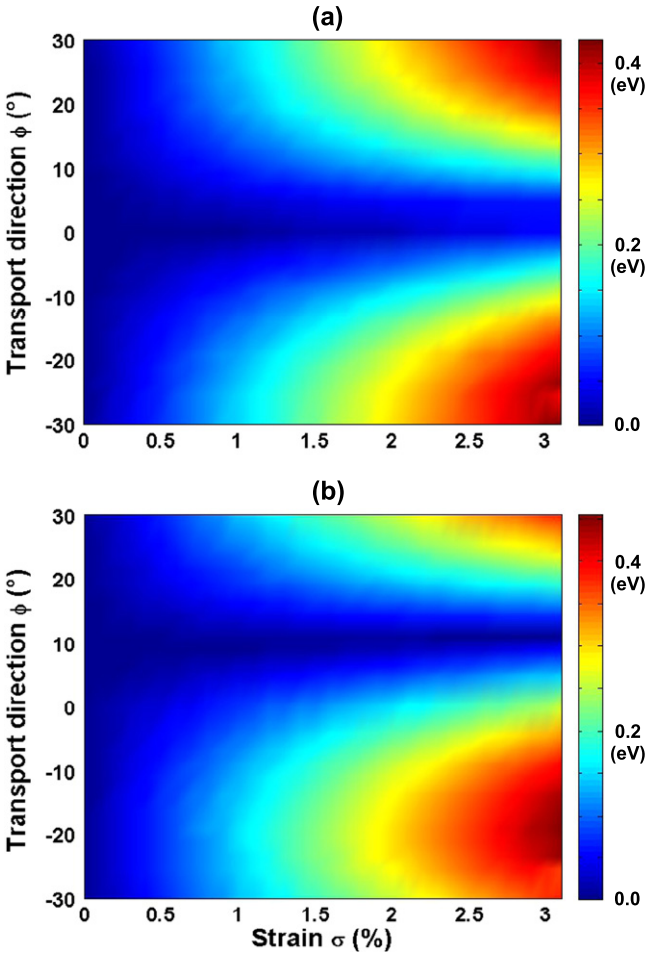

Figure 8. Maps showing the conduction gap as a function of shear strain (a) and combined strain (b) with different transport directions ϕ.

conduction gap for $\phi = 30°$, compared to the case of $\phi = 0$, as mentioned. Again, we found the same qualitative behavior of the conduction gap when applying the strains of $\{\sigma, \theta\}$ and $\{-\sigma, \theta + 90°\}$.

We now investigate the conduction gap with respect to different transport directions ϕ. We display a (θ, ϕ)-map of conduction gap for $\sigma = 4\%$ in figure 6 together with an additional diagram, in the top, illustrating the rotation of Dirac points in the k-space with change in transport direction. It is clearly shown that (i) a similar scale of conduction gap is obtained for all different transport directions, (ii) there is a smooth and continuous shift of $E_{cond.gap} - \theta$ behavior when varying ϕ, and (iii) the same behavior of $E_{cond.gap}$ is also observed when comparing the two transport directions of ϕ and $\phi + 30°$, similar to the comparison for the case of $\phi = 0°$ and 30°. The data plotted in figure 6 additionally shows that $E_{cond.gap}$ takes the same value in both cases of $\{\phi, \theta\}$ and $\{-\phi, -\theta\}$ with a remark that the strains of $-\theta$ and $180° - \theta$ are identical. Moreover, the relationship between the values of θ and ϕ at peak or zero conduction gaps is almost linear. For instance, the relationship for conduction gap peaks is approximately given by $\theta = \theta_A - \eta_s \phi$. For tensile strains, η_s takes the values of ∼1.5667 and 1.4333 for two peaks at $\theta_A = 0$ and 90°, respectively. On the opposite, it is about 1.4333 and 1.5667 for $\theta_A = 0$ and 90°, respectively, in the case of compressive strains. All these features are essentially consequences of the rotation of Dirac points in the k-space with respect to the transport direction ϕ as illustrated in the diagram on the top of figure 6 and of the lattice symmetry of graphene.

As an alternative, we investigate another kind of strained junctions based on compressive and tensile-strained graphene sheets. The idea is that in this type of strained junction, the shifts of the Dirac points are different in two graphene sections of different strains, which offers the possibility of using smaller strains to achieve a similar conduction gap, compared to the case of unstrained/strained junctions. In figure 7, we display the maps of the conduction gap with respect to the directions of compressive (θ_c) and tensile (θ_t) strains in two cases of transport direction: $\phi = 0$ (armchair) and 30° (zigzag) for given strain strengths. Indeed, as seen in figures 7(a) and (b), with smaller strains $\{\sigma_c, \sigma_t\} = \{-2\%, 2\%\}$ or $\{-1\%, 3\%\}$, similar conduction gap of about 310 meV can be achieved while it requires a strain of 4% in the unstrained/strained junctions studied above. However, since the shift of the Dirac points is strongly dependent on the direction of applied strains and the transport direction, the properties of conduction gap in this case are more complicated. In particular, our calculations show that the preferred transport directions to achieve large conduction gaps are close to the armchair one. Otherwise, the conduction gap is generally smaller, similarly to the data for $\phi = 30°$ compared to $\phi = 0$, as displayed in figure 7. Additionally, the preferred directions of applied strains for $\phi = 0$ are $\theta_c = \theta_t = 0$ or 90°.

In addition to the uniaxial strains studied above, we notice that generally, the conduction gap can occur in any strained junction and, of course, is strongly dependent on the type of strain. As an illustration, we display in figure 8 the maps showing the dependence of the conduction gap on the strain and the transport direction for two strain models: pure shear strain [figure 8(a)] and combined uniaxial-shear strain [figure 8(b)]. The strain tensor has the form [26] $M_{ij}^{shear} = \sigma(\delta_{ix}\delta_{jy} + \delta_{iy}\delta_{jx})$ for shear strains and $M_{ij}^{comb} = \sigma(\delta_{ix}\delta_{jx} + \delta_{ix}\delta_{jy} + \delta_{iy}\delta_{jx})$ for combined strains. It is shown that compared to uniaxial strain cases, (i) it requires smaller shear (or combined) strains to achieve the same conduction gap and (ii) its dependence on the transport direction is very different. The former is consistent with the fact that the threshold deformation required to achieve a finite bandgap in graphene is lower for shear/combined strains than for a uniaxial strain [26, 27], because the similar difference between the three nearest $C - C$ bond lengths ($r_{1,2,3}$) can be obtained with weaker shear/combined strains. Regarding the transport-direction dependence, the shear strain gives a peak conduction gap at $\phi \simeq \pm 30°$ (zigzag) and a zero gap at $\phi \simeq 0$ (armchair directions). In contrast, for a uniaxial strain with

$\theta = 0$, the conduction gap is zero and maximum for the zigzag and armchair transport directions, respectively. In the case of combined strains, it has a peak at $\phi \simeq -20°$ and a zero value at $\phi \simeq 10°$. We would like to emphasize an additional point that the 'bandstructure analysis' used in this work is a simple and efficient way to calculate the conduction gap in these types of graphene junctions with different strain models.

Finally, we have one remark that, based on the analogy between strain and magnetic field for generating the shift of Dirac points in graphene, one might expect to achieve the same effects by creating a junction of graphene sections having different vector potentials, e.g., using a ferromagnetic stripe on top of graphene. However, previous studies in the literature have shown that to obtain the same effects as with a strain of a few percent, very large magnetic fields, i.e., from a few tens to hundreds Teslas [36, 48, 49], are required, making it very difficult to be realized in practice. Therefore, the strain could be a more realistic technique to achieve a finite conduction gap in this type of junctions.

4. Conclusion

Based on tight-binding calculations, we have investigated the strain effects on the transport properties of graphene-strained junctions and discussed systematically the possibility of achieving a large conduction gap with respect to the strain strength, its applied direction and the transport direction. It has been shown that due to the strain-induced displacement of Dirac cones away from the *K*-point, a finite conduction gap higher than 500 meV can be achieved for a uniaxial strain of only 6%. However, since it is essentially due to the shift of Dirac points along the k_y-axis, this conduction gap is strongly dependent not only on the strain strength, but also on the direction of applied strain and the transport direction. As an important result of the work, a full picture of these properties of the conduction gap has been presented and explained. The study could be a useful guide and provides an efficient calculation method for the investigation of graphene-strained junctions in electronic applications, e.g., as recently proposed in [43], and for other applications as strain sensors.

Acknowledgements

This research in Hanoi is funded by Vietnam's National Foundation for Science and Technology Development (NAFOSTED) under grant number 103.02–1012.42. We also acknowledges the French ANR for financial support under the project MIGRAQUEL (Grant no. ANR-10-BLAN-0304).

References

[1] Castro Neto A H, Guinea F, Peres N M R, Novoselov K S and Geim A K 2009 *Rev. Mod. Phys.* **81** 109
[2] Schwierz F 2010 *Nat. Nanotechnol.* **5** 487
[3] Wu Y, Farmer D B, Xia F and Avouris P 2013 *Proc. IEEE* **101** 1620
[4] Bolotin K I, Sikes K J, Jiang J, Klima M, Fudenberg G, Hone J, Kim P and Stormer H L 2008 *Solid State Commun.* **146** 351
[5] Zomer P J, Dash S P, Tombros N and van Wees B J 2011 *Appl. Phys. Lett.* **99** 232104
[6] Novoselov K S, Geim A K, Morozov S V, Jiang D, Zhang Y, Dubonos S V, Grigorieva I V and Firsov A A 2004 *Science* **306** 666
[7] Wu Y *et al* 2012 *Nano Lett.* **12** 3062
[8] Cheng R, Bai J, Liao L, Zhou H, Chen Y, Liu L, Lin Y C, Jiang S, Huang Y and Duan X 2012 *Proc. Nat. Acad. Sci. USA* **109** 11588
[9] Guo Z *et al* 2013 *Nano Lett.* **13** 942
[10] Meric I, Han M Y, Young A F, Ozyilmaz B, Kim P and Shepard K L 2008 *Nat. Nanotechnol.* **3** 654
[11] Han M Y, Ozyilmaz B, Zhang Y and Kim P 2007 *Phys. Rev. Lett.* **98** 206805
[12] Kharche N and Nayak S K 2011 *Nano Lett.* **11** 5274
[13] Lherbier A, Botello-Mendez A R and Charlier J-C 2013 *Nano Lett.* **13** 1446
[14] Bai J, Zhong X, Jiang S, Huang Y and Duan X 2010 *Nat Nanotechnol.* **5** 190
[15] Berrada S, Hung Nguyen V, Querlioz D, Saint-Martin J, Alarcón A, Chassat C, Bournel A and Dollfus P 2013 *Appl. Phys. Lett.* **103** 183509
[16] Zhang Y, Tang T T, Girit C, Hao Z, Martin M C, Zettl A, Crommie M F, Ron Shen Y and Wang F 2009 *Nature* **459** 820
[17] Querlioz D, Apertet Y, Valentin A, Huet K, Bournel A, Galdin-Retailleau S and Dollfus P 2008 *Appl. Phys. Lett.* **92** 042108
[18] Hung Nguyen V, Chung Nguyen M, Viet Nguyen H and Dollfus P 2013 *J. Appl. Phys.* **113** 013702
[19] Fiori G and Iannaccone G 2009 *IEEE Electron Device Lett* **30** 261
[20] Sharma B K and Ahn J-H 2013 *Solid State Electron.* **89** 177
[21] Kim K S, Zhao Y, Jang H, Lee S Y, Kim J M, Kim K S, Ahn J-H, Kim P, Choi J-Y and Hong B H 2009 *Nature* **457** 706
[22] Garza H H P, Kievit E W, Schneider G F and Staufer U 2014 *Nano Lett.* **14** 4107
[23] Shioya H, Craciun M F, Russo S, Yamamoto M and Tarucha S 2014 *Nano Lett.* **14** 1158
[24] Pereira V M and Neto A H Castro 2009 *Phys. Rev. Lett.* **103** 046801
[25] Lu Y and Guo J 2010 *Nano Res.* **3** 189
[26] Cocco G, Cadelano E and Colombo L 2010 *Phys. Rev.*B **81** 241412
[27] Pereira V M, Castro Neto A H and Peres N M R 2009 *Phys. Rev.*B **80** 045401
[28] Ni Z H, Yu T, Lu Y H, Wang Y Y, Feng Y P and Shen Z X 2008 *ACS Nano* **2** 2301
Ni Z H, Yu T, Lu Y H, Wang Y Y, Feng Y P and Shen Z X 2009 *ACS Nano* **3** 483 erratum
[29] Huang M, Yan H, Heinz T F and Hone J 2010 *Nano Lett.* **10** 4074
[30] Bunch J S, van der Zande A M, Verbridge S S, Frank I W, Tanenbaum D M, Parpia J M, Craighead H G and McEuen P L 2007 *Science* **315** 490
[31] Bala Kumar S and Guo J 2012 *Nano Lett.* **12** 1362
[32] Pereira V M, Castro Neto A H, Liang H Y and Mahadevan L 2010 *Phys. Rev. Lett.* **105** 156603
[33] Pellegrino F M D, Angilella G G N and Pucci R 2010 *Phys. Rev.*B **81** 035411
[34] Pereira V M, Ribeiro R M, Peres N M R and Neto A H Castro 2010 *Europhys. Lett.* **92** 67001
[35] Ni G-X, Yang H-Z, Ji W, Baeck S-J, Toh C-T, Ahn J-H, Pereira V M and Özyilmaz B 2014 *Adv. Mater.* **26** 1081

[36] Guinea F, Katsnelson M I and Geim A K 2010 *Nat.Phys.* **6** 30
[37] Low T and Guinea F 2010 *Nano Lett.* **10** 3551
[38] Zhai F and Yang L 2011 *Appl. Phys. Lett.* **98** 062101
[39] Lu Y and Guo J 2010 *App. Phys. Lett.* **97** 073105
[40] Fujita T, Jalil M B A and Tan S G 2010 *Appl. Phys. Lett.* **97** 043508
[41] de Juan F, Cortijo A, Vozmediano M A H and Cano A 2011 *Nat. Phys* **7** 810
[42] Bahamon D A and Pereira V M 2013 *Phys. Rev.* B **88** 195416
[43] Hung Nguyen V, Viet Nguyen H and Dollfus P 2014 *Nanotechnology* **25** 165201
[44] Blakslee O L, Proctor D G, Seldin E J, Spence G B and Weng T 1970 *J. Appl. Phys.* **41** 3373
[45] Hung Nguyen V, Mazzamuto F, Saint-Martin J, Bournel A and Dollfus P 2012 *Nanotechnology* **23** 065201
[46] Hasegawa Y, Konno R, Nakano H and Kohmoto M 2006 *Phys. Rev.*B **74** 033413
[47] Kitt A L, Pereira V M, Swan A K and Goldberg B B 2012 *Phys. Rev.*B **85** 115432
Kitt A L, Pereira V M, Swan A K and Goldberg B B 2013 *Phys. Rev.*B **87** 159909
[48] Levy N, Burke S A, Meaker K L, Panlasigui M, Zettl A, Guinea F, Castro Neto A H and Crommie M F 2010 *Science* **329** 544
[49] Lu J, Castro Neto A H and Loh K Ping 2012 *Nat. Commun.* **3** 823